the present study indicated that high plasma NA or Adr hardly affected the dynamic sympathetic neural regulation of HR in anesthetized rabbits.

MATERIALS AND METHODS

Animal preparation. The animals were cared for in strict accordance with the Guiding Principles for the Care and Use of Animals in the Field of Physiological Sciences approved by the Physiological Society of Japan. Eighteen Japanese white rabbits weighing from 2.4 to 3.2 kg were anesthetized by a mixture of α-chloralose (40 mg/ml) and urethane (250 mg/ml), initiated with a bolus injection of 2 ml/kg and maintained with a continuous administration at 0.5 ml·kg^{-1}·h^{-1}. The rabbits were intubated and mechanically ventilated with oxygen-enriched room air. The right cardiac postganglionic sympathetic nerve was identified in the right thoracic cavity and sectioned. Usually, HR dropped immediately after the sectioning of the right cardiac sympathetic nerve, suggesting the importance of the right cardiac sympathetic nerve in determining baseline HR. A pair of platinum electrodes was attached to the cardiac end of the sectioned nerve for stimulation. The nerve and electrodes were secured by silicone glue (Kwik-Sil, World Precision Instruments, Sarasota, FL, USA). The left cardiac sympathetic nerve and other sympathetic branches to the heart were kept intact. The carotid sinus nerves and aortic depressor nerves were sectioned bilaterally to minimize changes in systemic sympathetic activity induced by baroreflexes. The vagal nerves were also sectioned bilaterally to eliminate the vagal effect on the heart. The vagotomy did not change HR significantly at this stage, possibly because of the vagolitic effects of the anesthesia. Arterial pressure (AP) was measured by a micromanometer (Millar Instruments, Houston, TX, USA) inserted into the thoracic aorta from the right femoral artery. HR was measured with a cardiotachometer (AT-601G, Nihon Kohden, Tokyo, Japan). An arterial catheter was inserted into the left femoral artery to sample blood for plasma catecholamine measurements. A double-lumen venous catheter was introduced into the right femoral vein for continuous anesthetic infusion and exogenous catecholamine administration.

Protocols. We quantified the dynamic sympathetic neural regulation of HR by using a transfer function analysis [3, 4]. To estimate the transfer function from cardiac SNS to HR, we dynamically stimulated the right cardiac sympathetic nerve as follows. The pulse duration was set at 2 ms, and the pulse amplitude was adjusted to obtain an HR increase of approximately 50 bpm (beats/min) during a 5-Hz constant stimulation in each animal. The resulting amplitude ranged from 0.8 to 2.0 V among animals. With these settings, the stimulation frequency was randomly assigned at either 0 or 5 Hz every 2 s, according to a binary white noise sequence (see appendix A for additional information). The average stimulation frequency was therefore 2.5 Hz. The input power spectral density of SNS was relatively flat up to 0.25 Hz.

In *Protocol 1* ($n = 6$), physiological saline was infused intravenously at 1 ml·kg^{-1}·h^{-1} for 30 min after the end of surgical preparation (Fig. 1). A 300-μl volume of arterial blood was sampled under control conditions (designated as NA_0 condition) for plasma catecholamine measurements. Following the blood sampling, dynamic SNS was applied for 15 min to estimate the transfer function from SNS to HR. Arterial blood was sampled during the last minute of dynamic SNS under the NA_0 condition. Next, 1-μg/ml NA solution was infused at 1 μg·kg^{-1}·h^{-1} (NA_1). Fifteen min after the initiation of NA_1 administration, when AP and HR had reached new steady states, arterial blood sampling and 15-min dynamic SNS were repeated. Third, a 10-μg/ml NA solution was administered at 10 μg·kg^{-1}·h^{-1} (NA_{10}). Fifteen min after the initiation of NA_{10} administration, arterial blood sampling and 15-min dynamic SNS were repeated.

In *Protocol 2* ($n = 6$), experimental procedures similar to those in *Protocol 1* were conducted, using the Adr solution instead of the NA solution. The transfer function from SNS to HR was estimated under control condition (designated as Adr_0 condition), as well as during the administration of 1-μg/ml Adr solution at 1 μg·kg^{-1}·h^{-1} (Adr_1) and 10-μg/ml Adr solution at 10 μg·kg^{-1}·h^{-1} (Adr_{10}).

In *Protocol 3* ($n = 6$), we examined the effects of an intravenous administration of a β-adrenergic agonist isoproterenol on the transfer function from SNS to HR. Using experimental procedures similar to those in *Protocol 1*, we

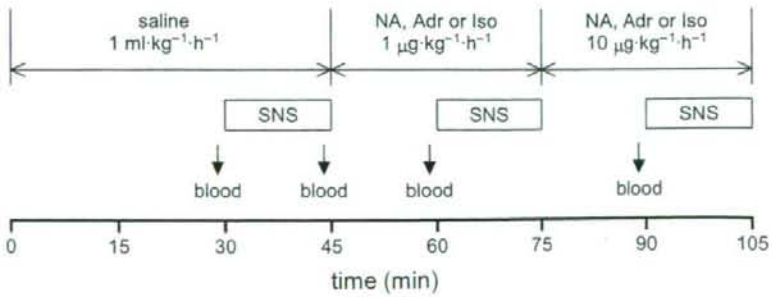

Fig. 1. Schematic diagram showing the experimental protocol. The downward arrows indicate the timings of blood sampling for catecholamine measurements (for *Protocols 1* and *2*). SNS: sympathetic nerve stimulation. NA: noradrenaline; Adr: adrenaline; Iso: isoproterenol.

administered 1-μg/ml isoproterenol solution at 1 μg·kg^{-1}·h^{-1} (Iso_1) and 10-μg/ml isoproterenol solution at 10 μg·kg^{-1}·h^{-1} (Iso_{10}) and estimated the transfer function under the control (designated as Iso_0), Iso_1, and Iso_{10} conditions.

Data analysis. The SNS command and HR were stored at a sampling rate of 200 Hz. The data were analyzed from only 2 min after the initiation of SNS to remove the initial trend of the HR increase. To estimate the transfer function from SNS to HR, we resampled the SNS-HR data pairs at 8 Hz. These data were segmented into 10 sets of half-overlapping bins of 1,024 data points each. In each segment, a linear trend was subtracted and a Hanning window was applied. The fast Fourier transform was then applied to obtain the frequency spectra of SNS and HR [9]. We calculated the ensemble averages of input power spectral density [$S_{SNS\cdot SNS}(f)$], output power spectral density [$S_{HR\cdot HR}(f)$], and cross-spectral density between the input and output [$S_{HR\cdot SNS}(f)$]. The transfer function [$H(f)$] was estimated using the following equation [10, 11].

$$H(f)=\frac{S_{HR\cdot SNS}(f)}{S_{SNS\cdot SNS}(f)} \tag{1}$$

We also calculated the magnitude-squared coherence function [$Coh(f)$] using the following equation [10, 11].

$$Coh(f)=\frac{\left|S_{HR\cdot SNS}(f)\right|^2}{S_{SNS\cdot SNS}(f)\,S_{HR\cdot HR}(f)} \tag{2}$$

The coherence function is a frequency-domain measure of the linear dependence between the input and output signals. A unity coherence value indicates a perfect linear dependence of HR on SNS, whereas a zero coherence value indicates the total independence between SNS and HR.

In *Protocols 1* and *2*, the transfer function from SNS to HR was parameterized by using a mathematical model [$H_m(f)$] of a second-order low-pass filter with pure dead time, using the following equation [3, 12].

$$H_m(f)=\frac{K}{1+2\zeta\frac{f}{f_N}j+\left(\frac{f}{f_N}j\right)^2}\exp(-2\pi f\,jL) \tag{3}$$

where K is the dynamic gain (in bpm/Hz), f_N is the natural frequency (in Hz), ζ is the damping ratio, and L is the pure dead time (in s); j represents the imaginary unit (see appendix B for details). A nonlinear iterative least square fitting was performed to minimize the following error function.

$$err=\frac{\sum_{i=1}^{N}\left|H(f_i)-H_m(f_i)\right|^2}{\sum_{i=1}^{N}\left|H(f_i)\right|^2},\quad f_i=f_0\times i \tag{4}$$

where f_0 indicates the fundamental frequency of the Fourier transform. N specifies the upper frequency bound of the fitting procedure. We set N at 32 so as to fit $H_m(f)$ to $H(f)$ up to 0.25 Hz.

In *Protocol 3*, because the transfer function from SNS to HR during Iso_{10} was significantly deviated from the mathematical model of a second-order low-pass filter with pure dead time (Eq. 3), we did not fit the mathematical model to the transfer function and adopted the transfer gain values at the lowest frequency ($G_{0.0078}$) and at 0.1 Hz ($G_{0.1}$) to represent the frequency response of HR to SNS.

Catecholamine measurements. The arterial blood sample was centrifuged and a 100-μl volume of plasma was obtained. The plasma was transferred into a 1.5-ml polypropylene conical tube. A 50-μl volume of the working internal standard solution [100 pg of 3,4-dihydroxybenzylamine (DHBA)], 5 mg of acid-washed alumina, and 1.0 ml of 1-M tris(hydroxymethyl) aminomethane buffer (pH 8.6), containing 0.2% disodium ethylendiaminetetraacetic acid (EDTA), was added to the conical tube and shaken for 15 min. After shaking, the alumina was washed three times with distilled water, transferred into a microfilter (Ultrafree C3, Millipore, Bedford, MA), and centrifuged to remove excess fluid. NA, Adr, and DHBA were then eluted from the alumina, using 60 μl of 2% acetic acid, and their concentrations were measured by using high-performance liquid chromatography with electrochemical detection (DTA-300, Eicom, Kyoto, Japan). Plasma NA and Adr concentrations were calculated, taking into account the recovery rate of DHBA.

Statistical analysis. All data are presented in mean and mean ± SEM values. In *Protocol 1*, the effect of dynamic SNS on the plasma NA concentration was examined by a paired t-test under NA_0 condition. The NA and Adr concentrations before SNS were compared among NA_0, NA_1, and NA_{10} conditions, using Dunnett's test against a single control following the repeated-measures analysis of variance [13]. We also compared mean HR, mean AP, and parameters of the transfer function among NA_0, NA_1, and NA_{10} conditions, using Dunnett's test following repeated-measures analysis of variance. In *Protocol 2*, the effect of dynamic SNS on the plasma Adr concentration was examined by a paired t-test under Adr_0 condition. Other values, including plasma NA and Adr concentrations, mean HR, mean AP, and parameters of the transfer function, were compared among Adr_0, Adr_1, and Adr_{10} conditions, using Dunnett's test following repeated-measures analysis of variance. In *Protocol 3*, mean HR, mean AP, and gain values ($G_{0.0078}$ and $G_{0.1}$) were compared among Iso_0, Iso_1,

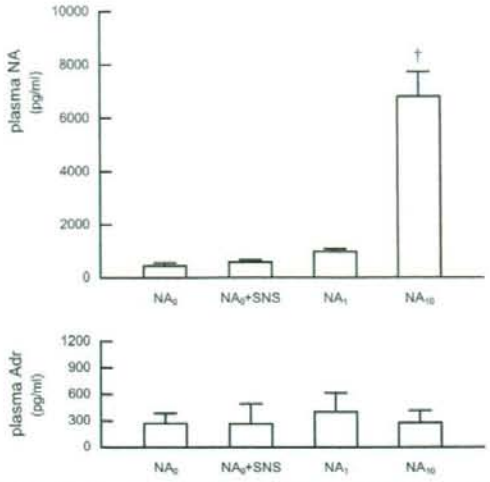

Fig. 2. Plasma concentrations of NA and Adr obtained from *Protocol 1*. The plasma NA concentration was significantly increased during the NA_{10} condition. The plasma Adr concentration was not changed significantly by the NA infusion. NA_0: saline infusion; NA_1 and NA_{10}: noradrenaline infusions at 1 and 10 $\mu g \cdot kg^{-1} \cdot h^{-1}$.

and Iso_{10} conditions, using Dunnett's test following repeated-measures analysis of variance. In all of the statistics, the difference was considered significant at $P < 0.05$.

RESULTS

Effects of high plasma NA on the dynamic sympathetic neural regulation of HR

In *Protocol 1*, dynamic SNS for 15 min did not change the plasma NA or Adr concentration significantly during NA_0 condition (Fig. 2, NA_0 vs. NA_0+SNS). The plasma NA concentration prior to dynamic SNS did not increase significantly during NA_1 condition, but increased to approximately 15 times higher during NA_{10} condition compared to NA_0 condition. The NA infusion did not significantly affect the plasma Adr concentration.

Figure 3A illustrates the time series of SNS, HR, and AP under NA_0, NA_1, and NA_{10} conditions obtained from one animal. The SNS was assigned at 0 or 5 Hz according to a binary white noise sequence. HR changed randomly in response to the dynamic SNS. Mean HR was slightly increased during NA infusion, whereas the amplitude of HR variation appeared unchanged. Mean AP was increased during NA_{10} condition compared to NA_0 condition.

Figure 3B shows averaged transfer functions from SNS to HR during NA_0, NA_1, and NA_{10} conditions obtained from all six animals in *Protocol 1*. The solid curve and the dashed curves in each plot represent mean and mean ± SEM values, respectively. In the gain plot, the transfer

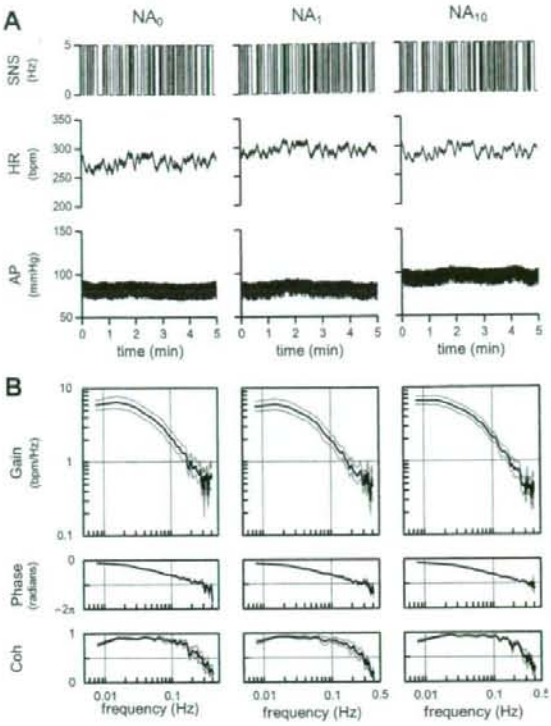

Fig. 3. A: Time series of one animal obtained from *Protocol 1*. Sympathetic nerve stimulation (SNS), heart rate (HR), and arterial pressure (AP) are shown. HR changed dynamically in response to SNS. **B**: Averaged transfer functions from SNS to HR during NA_0, NA_1, and NA_{10} conditions obtained from *Protocol 1* ($n = 6$). NA infusion did not affect the transfer function significantly except for changes in the damping ratio. Solid and dashed curves indicate mean and mean ± SEM values, respectively.

gain decreased with increasing frequency, reflecting the low-pass characteristics of the sympathetic neural regulation of HR. In the phase plot, the phase was near zero radians at the lowest frequency and delayed with increasing frequency, reflecting the SNS increases of HR. In the coherence plot, high coherence values up to 0.2 Hz indicate that approximately 80% of the HR variation in this frequency range was explained by the linear dynamics between SNS and HR. The transfer functions were similar among the three conditions. The dynamic gain, natural frequency, and pure dead time did not differ among the three conditions (Table 1). However, the damping ratio was significantly greater during NA_1 and NA_{10} conditions compared to the NA_0 condition.

Mean HR before SNS did not differ among NA_0, NA_1, and NA_{10} conditions, whereas mean HR during SNS increased significantly during NA_1 and NA_{10} conditions compared to NA_0 condition (Table 1). Although the repeated-measures analysis of variance indicated that the ef-

Table 1. Parameters obtained from *Protocol 1*.

	NA_0	NA_1	NA_{10}
HR, bpm			
Before SNS	248 ± 20	250 ± 19	251 ± 20
During SNS	280 ± 24	289 ± 22**	288 ± 22**
AP, mmHg			
Before SNS	95.7 ± 7.2	99.3 ± 8.1	106.6 ± 6.6*
During SNS	93.6 ± 8.0	102.9 ± 8.8**	106.0 ± 7.0**
Dynamic gain (K), bpm/Hz	7.6 ± 1.2	7.5 ± 1.1	8.1 ± 1.1
Natural frequency (f_N), Hz	0.080 ± 0.010	0.084 ± 0.010	0.083 ± 0.010
Damping ratio (ζ)	1.16 ± 0.05	1.48 ± 0.03*	1.52 ± 0.11*
Pure dead time (L), s	0.44 ± 0.08	0.55 ± 0.07	0.52 ± 0.06
Fitting error (err), %	1.6 ± 0.3	2.2 ± 0.6	1.6 ± 0.4

Values are means ± SEM. **$P < 0.01$ and *$P < 0.05$ vs. the corresponding value obtained during NA_0 condition. HR: heart rate. AP: arterial pressure. SNS: sympathetic nerve stimulation.

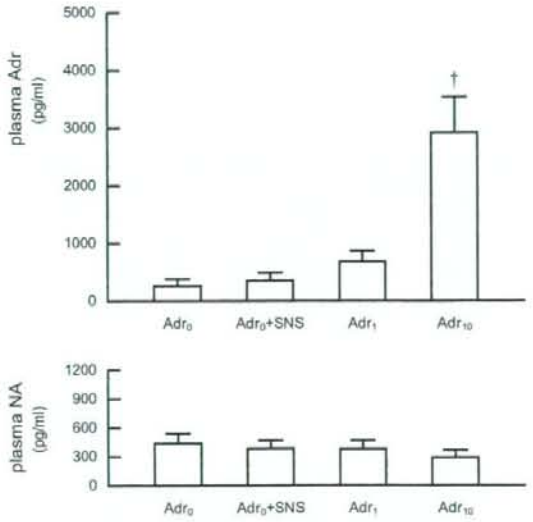

Fig. 4. Plasma concentrations of Adr and NA obtained from *Protocol 2*. The plasma Adr concentration was significantly increased during the Adr_{10} condition. The plasma NA concentration was not changed significantly by Adr infusion. Adr_0: saline infusion; Adr_1 and Adr_{10}: adrenaline infusions at 1 and 10 μg·kg⁻¹·h⁻¹.

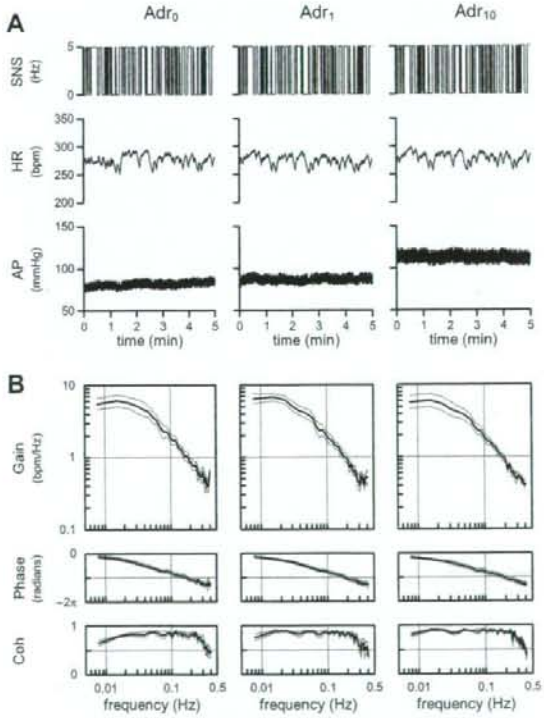

Fig. 5. A: Time series of one animal obtained from *Protocol 2*. HR changed dynamically in response to SNS. **B**: Averaged transfer functions from SNS to HR during Adr_0, Adr_1, and Adr_{10} conditions obtained from *Protocol 2* ($n = 6$). Adr infusion did not affect the transfer function significantly. Solid and dashed curves indicate mean and mean ± SEM values, respectively.

fects of NA infusion on mean HR during SNS were significant, the magnitude of the HR increase was small relative to the interindividual variation of HR. Mean AP before SNS was significantly elevated during NA_{10} condition, but not during NA_1 condition compared to NA_0 condition. Mean AP during SNS was increased significantly during both NA_1 and NA_{10} conditions compared to NA_0 condition.

Table 2. Parameters obtained from *Protocol 2*.

	Adr_0	Adr_1	Adr_{10}
HR, bpm			
Before SNS	231 ± 12	232 ± 10	228 ± 7
During SNS	274 ± 13	275 ± 13	274 ± 13
AP, mmHg			
Before SNS	93.1 ± 9.7	99.0 ± 8.3	113.7 ± 5.2**
During SNS	101.3 ± 8.0	103.8 ± 8.4	116.6 ± 4.6**
Dynamic gain (K), bpm/Hz	8.0 ± 0.6	8.4 ± 0.8	8.2 ± 1.0
Natural frequency (f_N), Hz	0.070 ± 0.005	0.071 ± 0.005	0.067 ± 0.006
Damping ratio (ζ)	1.09 ± 0.20	1.32 ± 0.11	1.39 ± 0.17
Pure dead time (L), s	0.55 ± 0.13	0.66 ± 0.09	0.63 ± 0.15
Fitting error (err), %	2.5 ± 0.5	1.8 ± 0.3	2.3 ± 0.6

Values are means ± SEM. **$P < 0.01$ vs. the corresponding value obtained during Adr_0 condition. HR: heart rate. AP: arterial pressure. SNS: sympathetic nerve stimulation.

Effects of high plasma Adr on the dynamic sympathetic neural regulation of HR

In *Protocol 2*, dynamic SNS for 15 min did not significantly change the plasma Adr or NA concentration during Adr_0 condition (Fig. 4, Adr_0 vs. Adr_0+SNS). The plasma Adr concentration prior to dynamic SNS did not increase significantly during Adr_1 condition, but increased to approximately 11 times higher during Adr_{10} condition compared to Adr_0 condition. The Adr infusion did not significantly affect the plasma NA concentration.

Figure 5A illustrates the time series of SNS, HR, and AP during Adr_0, Adr_1, and Adr_{10} conditions obtained from one animal. HR changed randomly in response to the dynamic SNS. The Adr infusion did not significantly change mean HR or the amplitude of HR variation among Adr_0, Adr_1, and Adr_{10} conditions. Mean AP increased during Adr_{10} condition compared to the Adr_0 condition.

Figure 5B shows averaged transfer functions from SNS to HR during Adr_0, Adr_1, and Adr_{10} conditions obtained from all of the six animals in *Protocol 2*. There seem to be no effects of Adr infusion on the transfer functions. No significant differences in dynamic gain, natural frequency, damping ratio, and pure dead time were observed among the three conditions (Table 2).

Mean HR did not differ significantly among Adr_0, Adr_1, and Adr_{10} conditions, both before and during SNS (Table 2). Mean AP increased significantly during Adr_{10} condition, but not during Adr_1 condition compared with Adr_0 condition, both before and during SNS.

Effects of intravenous isoproterenol on the dynamic sympathetic neural regulation of HR

Figure 6A illustrates the time series of SNS, HR, and AP during Iso_0, Iso_1, and Iso_{10} conditions obtained from one animal. HR changed randomly in response to the dynamic SNS under the Iso_0 condition. Although the dynamic HR response to SNS was maintained under the Iso_1 condition, mean HR was significantly elevated, and no apparent HR response was observed under the Iso_{10} condition.

Figure 6B shows averaged transfer functions from SNS to HR during Iso_0, Iso_1, and Iso_{10} conditions obtained from all of the six animals in *Protocol 3*. The transfer function showed a slight downward shift under the Iso_1 condition compared to the Iso_0 condition. It was significantly deformed and lost consistent characteristics across the animals under the Iso_{10} condition, as evidenced by large standard errors (dashed lines). The gain values ($G_{0.0078}$ and $G_{0.1}$) were significantly lower under the Iso_{10} condition compared to the Iso_0 condition (Table 3).

Mean HR did not change significantly under the Iso_1 condition, but increased significantly under the Iso_{10} condition compared to that under the Iso_0 condition, both before and during SNS (Table 3). Mean AP before SNS was significantly increased under the Iso_1 condition, but not under the Iso_{10} condition compared to that under the Iso_0 condition. Mean AP during SNS did not differ under the Iso_1 condition, but decreased significantly under the Iso_{10} condition compared to that under the Iso_0 condition.

DISCUSSION

We have examined the effects of high plasma NA or Adr on the transfer function from SNS to HR and found that high plasma catecholamines within physiological limits (approximately 10 times the resting levels) were ineffective to alter the sympathetic neural regulation of HR. Although the baseline HR was higher than the resting HR reported in conscious rabbits, the high baseline HR may be partly due to vagotomy. Because dynamic SNS (average stimulation frequency was 2.5 Hz) could increase mean HR, on the average, by 32 bpm in *Protocol 1* and by 43 bpm in *Protocol 2* under control conditions (NA_0 and Adr_0), the insignificant effects of high plasma catecholamines on HR cannot be explained by a simple saturation

Table 3. Parameters obtained from *Protocol 3*.

	Iso_0	Iso_1	Iso_{10}
HR, bpm			
Before SNS	244 ± 7	245 ± 6	289 ± 8**
During SNS	278 ± 11	280 ± 10	293 ± 9**
AP, mmHg			
Before SNS	80.2 ± 8.5	96.2 ± 4.9*	83.5 ± 7.1
During SNS	90.9 ± 7.4	93.1 ± 7.4	82.9 ± 7.0**
$G_{0.0078}$, bpm/Hz	5.9 ± 1.0	4.7 ± 0.8	1.0 ± 0.4**
$G_{0.1}$, bpm/Hz	1.3 ± 0.3	0.9 ± 0.2	0.2 ± 0.2**

Values are means ± SEM. $^{**}P < 0.01$ and $^{*}P < 0.05$ vs. the corresponding value obtained during Iso_0 condition. HR: heart rate. AP: arterial pressure. SNS: sympathetic nerve stimulation. $G_{0.0078}$: transfer gain value at 0.0078 Hz. $G_{0.1}$: transfer gain value at 0.1 Hz.

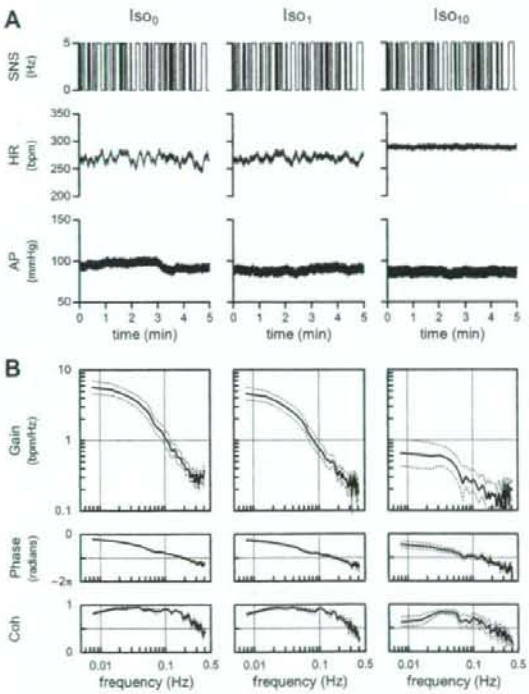

Fig. 6. A: Time series of one animal obtained from *Protocol 3*. Although HR changed dynamically in response to SNS under Iso_0 and Iso_1 conditions, mean HR elevated significantly, and no apparent dynamic HR response was observed under the Iso_{10} condition. **B**: Averaged transfer functions from SNS to HR during Iso_0, Iso_1, and Iso_{10} conditions obtained from *Protocol 3* (n = 6). The transfer gain reduced significantly and varied among animals, as evidenced by the large SEM under the Iso_{10} condition. Solid and dashed curves indicate mean and mean ± SEM values, respectively. Iso_0: saline infusion; Iso_1 and Iso_{10}: isoproterenol infusions at 1 and 10 $\mu g \cdot kg^{-1} \cdot h^{-1}$.

phenomenon of the HR response to catecholamines or by complete downregulation of β-adrenergic receptors under the present experimental settings. Actually, we confirmed that the same dose of intravenous administration of a β-adrenergic agonist isoproterenol increased mean HR significantly and blunted the transfer function (Fig. 6, Iso_{10} in *Protocol 3*). It is quite likely that NA released from the sympathetic nerve terminals during SNS has much stronger effects on HR in comparison with circulating catecholamines.

Effects of high plasma NA on the sympathetic neural regulation of HR

The plasma NA concentration increased approximately 15 times higher during NA_{10} condition than during NA_0 condition. Nevertheless, mean HR before SNS did not change significantly during NA_{10} condition compared to NA_0 condition (Table 1). In contrast, mean AP before SNS increased significantly during NA_{10} condition compared to NA_0 condition (Table 1). Young *et al.* [14] also reported an increase in AP and no changes in HR during NA infusion at 0.2 $\mu g \cdot kg^{-1} \cdot min^{-1}$ (12 $\mu g \cdot kg^{-1} \cdot h^{-1}$) in conscious dogs, though the baroreflexes could have counteracted the potential increase of HR in their study. These results indicate that the vascular bed is more responsive to plasma NA than the sinus node. A tighter synaptic cleft of the neuroeffector junction of the cardiac muscle compared to the vasculature, though it was reported in rat tissues [15], might explain the differential sensitivity to plasma NA between HR and AP.

Cardiac SNS significantly increased the mean HR without increasing the plasma NA concentration (Fig. 2), consistent with previous studies in anesthetized dogs [16] and cats [17]. Although mean HR before SNS did not differ among NA_0, NA_1, and NA_{10} conditions, mean HR during SNS was significantly higher during NA_1 and NA_{10} conditions compared to control (Table 1). These results are in opposition to the hypothesis that high plasma NA activates presynaptic α_2-adrenergic receptors and attenuates the HR response to SNS. One possible explanation for the increased mean HR during SNS under conditions of the NA infusion is as follows. NA released from the sympathetic nerve terminals is removed from the synaptic cleft by two catecholamine uptake mechanisms: a high-affinity, low-capacity neuronal uptake ($uptake_1$) and a low-affinity, high-capacity extraneuronal uptake ($uptake_2$) [5,

18, 19]. The uptake$_1$ mechanism also contributes to plasma clearance of NA [20]. High plasma NA might occupy the uptake$_1$ process to some extent and slow the NA removal from the synaptic cleft during SNS. As a result, the positive chronotropic effects of SNS might be augmented. Honda *et al.* [8] investigated the relationship between the kinetics of plasma catecholamines and cardiac sympathetic nerve activity during systemic hypotension induced by vena cava occlusion. They showed that the cardiac uptake of NA proportionally increased as the arterial NA concentration increased and that there was a negative correlation between the cardiac uptake of NA and the percent increase in mean cardiac sympathetic nerve activity. The negative correlation between the cardiac uptake of NA and the percent increase in mean cardiac sympathetic nerve activity might support the notion that NA of plasma origin and that of neural origin share the uptake$_1$ process. Although the within-individual change was statistically significant, the magnitude of HR increase during SNS was small compared to the interindividual variation of mean HR. Therefore the augmentation of the positive chronotropic effects by high plasma NA may be physiologically insignificant.

In the transfer function parameters, the damping ratio alone was significantly increased during NA_1 and NA_{10} conditions compared with NA_0 condition (Table 1). As already discussed, high plasma NA might have interfered with the uptake$_1$ process and consequently changed the damping ratio of the transfer function [12]. The damping ratio is an important determinant of the system behavior of the second-order low-pass filter. Depending on the value of the damping ratio, the system behaves as underdamped ($0 < \zeta < 1$), critically damped ($\zeta = 1$), or overdamped ($\zeta > 1$) (see appendix B). In the present study, however, the damping ratios changed only from 1.2 to 1.5; thus the system should behave as over-damped under any of the NA_0, NA_1, and NA_{10} conditions. Given that other transfer function parameters including the dynamic gain, natural frequency, and pure dead time did not change significantly, high plasma NA has limited effects on the transfer function from SNS to HR.

Effects of high plasma Adr on the sympathetic neural regulation of HR

The plasma Adr concentration during Adr_{10} condition increased to approximately 11 times that during Adr_0 condition. Although high plasma Adr did not increase HR, it did increase AP (Table 2). In contrast, Young *et al.* [14] reported that an administration of Adr at 0.2 $\mu g \cdot kg^{-1} \cdot min^{-1}$ (12 $\mu g \cdot kg^{-1} \cdot h^{-1}$) significantly increased both AP and HR in conscious dogs. Since the plasma Adr concentration in their study increased to a similar degree to the present result, the HR response to plasma Adr may differ between rabbits and dogs. Other factors that potentially explain the discrepancy are the vagotomy and anesthesia used in the present study. On the other hand, the Adr administration could have altered cardiac sympathetic neural outflow in the study by Young *et al.* [14].

In the present experimental conditions, high plasma Adr did not increase mean HR during SNS compared to Adr_0 condition and did not affect the transfer function from SNS to HR either (Table 2). These results are in opposition to the hypothesis that high plasma Adr activates presynaptic β_2-adrenergic receptors and augments the HR response to SNS. Moreover, because Adr has lower affinity to the uptake$_1$ process compared to NA [18, 19], high plasma NA but not Adr affected the mean HR during SNS and the damping ratio of the transfer function via the mechanism of modulating the NA removal.

The present results are consistent with the study of Boudreau *et al.* [21], in which a 10-min administration of Adr (92 $ng \cdot kg^{-1} \cdot min^{-1}$ or 5.5 $\mu g \cdot kg^{-1} \cdot h^{-1}$) did not increase the NA release in response to cardiac SNS in anesthetized dogs. However, Boudreau *et al.* [21] also demonstrated that a 180-min administration of Adr did increase the NA release in response to cardiac SNS, along with an increased Adr level in the cardiac tissue. Plasma Adr can be taken up into the sympathetic nerve terminals and then coreleased with NA [22]. When Adr is coreleased with NA into the synaptic cleft, NA release may be facilitated via the presynaptic β_2-adrenergic mechanism because Adr is a more potent agonist for β_2-adrenergic receptors than NA [23]. Although the long-term effects of high plasma Adr on the transfer function from SNS to HR was not examined in the present study, it is conceivable that high plasma Adr does not affect the sympathetic neural regulation of HR unless the Adr accumulation in the sympathetic nerve terminals reaches a concentration that is high enough.

Effects of intravenous isoproterenol on the dynamic sympathetic neural regulation of HR

As expected, an intravenous administration of isoproterenol at 10 $\mu g \cdot kg^{-1} \cdot h^{-1}$ increased mean HR significantly both before and during SNS. The transfer gain of the HR response to SNS was significantly decreased under the Iso_{10} condition (Table 3). These results are similar to our previous finding that an increase in mean stimulation frequency of SNS increased mean HR and decreased the transfer gain [12]. We have explained a bidirectional augmentation of the dynamic HR response to autonomic nerve stimulation by using a nonlinear sigmoidal relationship between the autonomic tone and HR [3, 24]. In that concept, the operating point of HR critically affects the transfer gain of the HR response to sympathetic or vagal nerve stimulation; i.e., deviation of the operating point from the center of the sigmoidal relationship decreases the tangential line of the sigmoid curve that relates to the transfer gain. Such operating-point dependence of the transfer gain may explain, at least in part, the decrease in

the transfer gain under the Iso_{10} condition.

Several limitations need to be addressed. First, we performed the experiment in anesthetized rabbits. Because the anesthesia would affect the autonomic tone, the results may not be directly applicable to conscious animals. However, because we cut and stimulated the right cardiac sympathetic nerve, changes in autonomic outflow associated with anesthesia might not have significantly affected the present results. Second, as already mentioned, species differences in HR response to catecholamines may exist. Whether high plasma catecholamines affect the dynamic sympathetic neural regulation of HR in animal species other than rabbits requires further investigations. Third, the duration of catecholamine administration prior to SNS was set at 15 min. Although this priming time was sufficient for AP and HR to reach new steady states, the effects of longer durations of high plasma catecholamines on the dynamic sympathetic neural regulation of HR remain to be investigated. And fourth, because we stimulated the cardiac postganglionic sympathetic nerve, the possible effects of high plasma catecholamines on sympathetic ganglionic transmission were excluded.

In conclusion, although plasma NA or Adr were increased to a level 10–15 times higher than the baseline level by exogenous administration, such high plasma NA or Adr did not significantly affect the dynamic sympathetic neural regulation of HR in anesthetized rabbits. Although humoral and neural factors are thought to regulate the cardiovascular system in concert, the neural factor appears to be much stronger than the humoral factor as far as the HR regulation is concerned.

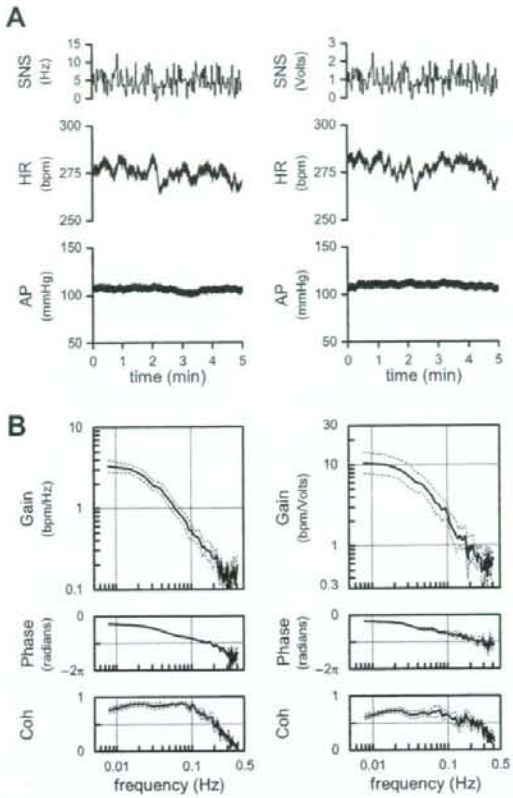

Fig. 7. A: Time series of SNS, HR, and AP using frequency modulation (left) and amplitude modulation (right) as the input signal. HR changed dynamically in response to both the frequency modulation and amplitude modulation of SNS. **B**: Averaged transfer functions obtained from 5 animals using frequency modulation (left) and amplitude modulation (right) as the input signal. Although the absolute gain values are different because of different units in inputs, the low-pass characteristics are in common for both transfer functions.

APPENDIX A

Frequency modulation versus amplitude modulation in nerve stimulation. Because the sinus node responds to NA released from the sympathetic nerve terminals and because the NA kinetics at the neuroeffector junction predominantly determine the low-pass filter characteristics of the HR response to SNS [12], whether the SNS is modulated by frequency or amplitude will not significantly affect the transfer function from SNS to HR. Although the frequency modulation and the amplitude modulation would reveal different nonlinear input-output relationships between the stimulation command signal and the number of nerve fibers actually discharged, a transfer function analysis using a white noise input can retrieve a linear input-output relationship even in the presence of a significant nonlinearity [11]. Although the SNS we used is different from a physiological discharge of nerve fibers, the HR response to physiological nerve discharge would obey the same principle characterized by the transfer function from SNS to HR. When we estimated the transfer function from recorded sympathetic nerve activity to HR, it also approximates to the second-order low-pass filter with pure dead time [25].

We compared the transfer function from SNS to HR identified by the frequency-modulation input and that by the amplitude-modulation input in 5 anesthetized rabbits. The left panel of Fig. 7A shows a typical time series of SNS, HR, and AP obtained from the frequency-modulation input with a constant amplitude of 3 V (2-ms pulse width, 2-s switching interval). The right panel of Fig. 7A shows the time series obtained from the amplitude-modulation input with a constant frequency of 5 Hz (2-ms pulse width, 2-s switching interval). Figure 7B summarizes the averaged transfer function obtained by the frequency-modulation input (left panel) and that by the amplitude-modulation input (right panel). Although the units of gain differ between the two, general low-pass characteristics were in common. The coherence values associated with

the amplitude-modulation input seems smaller than those associated with the frequency-modulation input. In regard to the amplitude-modulation input, the stimulation amplitude usually crosses the threshold amplitude, below which the nerve fibers do not discharge. Such a nonlinear process of the amplitude-modulation input would contribute to the lower coherence values.

APPENDIX B

A mathematical modeling of dynamic heart rate response to sympathetic nerve stimulation using a second-order low-pass filter with pure dead time. We adopted a mathematical model of a second-order low-pass filter with pure dead time to quantify the transfer function from SNS to HR. In the left panel of Fig. 8, the thick line represents a typical transfer function obtained under the NA_0 condition in one animal. The thin smooth curve represents a best-fit mathematical model. A schematic explanation of the model parameters is shown in the right panel of Fig. 8. The dynamic gain, K, determines the value the transfer gain approaches as the frequency goes to zero. The natural frequency, f_N, determines the frequency of low-pass characteristics. The phase of the second-order low-pass filter delays by $\pi/2$ radians at f_N when the pure dead time is zero. The damping ratio, ζ, determines how fast the transfer gain wanes around f_N. As an example, the gain plot shows a slight peaking around f_N when $\zeta = 0.5$. On the other hand, the gain plot shows a more gradual decrease around f_N when $\zeta = 2.0$. The maximum phase delay of the second-order low-pass filter is π radians. The pure dead time, L, determines the additional phase delay necessary for explaining the phase difference between the measured transfer function and the second-order low-pass filter.

This study was supported by "Health and Labour Sciences Research Grant for Research on Advanced Medical Technology" from the Ministry of Health, Labour and Welfare of Japan; "Health and Labour Sciences Research Grant for Research on Medical Devices for Analyzing, Supporting and Substituting the Function of Human Body" from the Ministry of Health, Labour and Welfare of Japan; "Health and Labour Sciences Research Grant H18-Iryo-Ippan-023" from the Ministry of Health, Labour and Welfare of Japan; "Program for Promotion of Fundamental Studies in Health Science" from the National Institute of Biomedical Innovation, a grant provided by the Ichiro Kanehara Foundation; "Ground-based Research Announcement for Space Utilization" promoted by the Japan Space Forum; and "Industrial Technology Research Grant Program in 03A47075" from the New Energy and Industrial Technology Development Organization (NEDO) of Japan.

REFERENCES

1. Kawada T, Fujiki N, Hosomi H. Systems analysis of the carotid sinus baroreflex system using a sum-of-sinusoidal input. Jpn J Physiol. 1992;42:15-34.
2. Kawada T, Yamamoto K, Kamiya A, Ariumi H, Michikami D, Shishido T, Sunagawa K, Sugimachi M. Dynamic characteristics of carotid sinus pressure-nerve activity transduction in rabbits. Jpn J Physiol. 2005;55:157-63.
3. Kawada T, Ikeda Y, Sugimachi M, Shishido T, Kawaguchi O, Yamazaki T, Alexander J Jr, Sunagawa K. Bidirectional augmentation of heart rate regulation by autonomic nervous system in rabbits. Am J Physiol Heart Circ Physiol. 1996;271:H288-95.
4. Kawada T, Sugimachi M, Shishido T, Miyano H, Ikeda Y, Yoshimura R, Sato T, Takaki H, Alexander J Jr, Sunagawa K. Dynamic vagosympathetic interaction augments heart rate response irrespective of stimulation patterns. Am J Physiol Heart Circ Physiol. 1997;272:H2180-7.
5. Cryer PE. Physiology and pathophysiology of the human sympathoadrenal neuroendocrine system. N Eng J Med. 1980;303:436-44.
6. Langer SZ, Adler-Graschinsky E, Giorgi O. Physiological significance of α-adrenoceptor-mediated negative feedback mechanism regulating noradrenaline release during nerve stimulation. Nature. 1977;265:648-50.
7. Majewski H, Rand MJ, Tung LH. Activation of prejunctional β-adrenoceptors in rat atria by adrenaline applied exogenously or released as a co-transmitter. Br J Pharmacol. 1981;73:669-79.
8. Honda T, Ninomiya I, Azumi T. Cardiac sympathetic nerve activity and catecholamine kinetics in cat hearts. Am J Pysiol Heart Circ Physiol. 1987;252:H879-85.
9. Brigham EO. The Fast Fourier Transform and Its Applications. Englewood Cliffs, NJ: Prentice-Hall; 1988. p. 167-203.
10. Bendat JS, Piersol AG. Random Data Analysis and Measurement Procedures. 3rd ed. New York: John Wiley & Sons; 2000. p. 189-217.
11. Marmarelis PZ, Marmarelis VZ. Analysis of Physiological Systems. New York: Plenum; 1978. p. 131-221.
12. Nakahara T, Kawada T, Sugimachi M, Miyano H, Sato T, Shishido T, Yoshimura R, Miyashita H, Inagaki M, Alexander J Jr, Sunagawa K. Neuronal uptake affects dynamic characteristics of heart rate response to sympathetic stimulation. Am J Physiol Regul Integr Comp Physiol. 1999;277:R140-6.
13. Glantz SA. Primer of Biostatistics (5th ed). New York: McGraw-Hill; 2002.
14. Young MA, Hintze TH, Vatner SF. Correlation between cardiac performance and

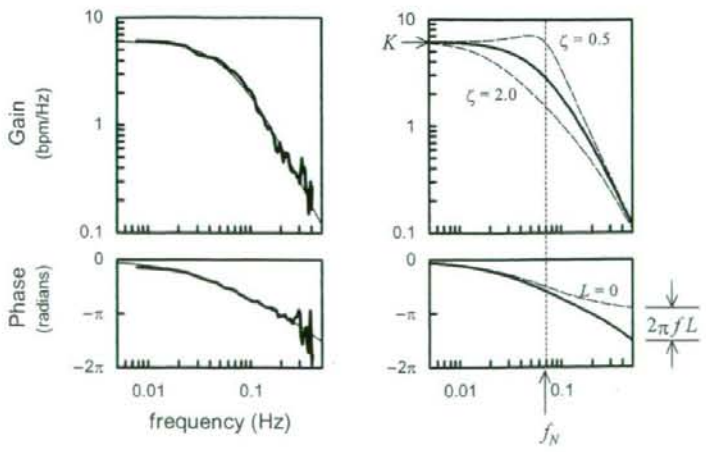

Fig. 8. A: Typical transfer function from SNS to HR obtained under control conditions (NA_0) in one animal. The thin smooth curve is a best-fit mathematical model for the transfer function. **B**: Schematic explanation of the model parameters. *K*: dynamic gain; f_N: natural frequency; ζ: damping ratio; *L*: pure dead time.

plasma catecholamine levels in conscious dogs. Am J Physiol Heart Circ Physiol. 1985;248:H82-8.
15. Novi AM. An electron microscope study of the innervation of papillary muscles in the rat. Anat Rec. 1968;160:123-41.
16. Yamaguchi N, de Champlain J, Nadeau R. Correlation between the response of the heart to sympathetic stimulation and the release of endogenous catecholamines into the coronary sinus of the dog. Circ Res. 1975;36:662-8.
17. Kawada T, Yamazaki T, Akiyama T, Shishido T, Miyano H, Sato T, Sugimachi M, Alexander J Jr, Sunagawa K. Interstitial norepinephrine level by cardiac microdialysis correlates with ventricular contractility. Am J Physiol Heart Circ Physiol. 1997;273:H1107-12.
18. Iversen LL. The uptake of catechol amines at high perfusion concentrations in the rat isolated heart: a novel catecholamine uptake process. Brit J Pharmacol. 1965;25:183-33.
19. Iversen LL. Uptake processes for biogenic amines. In: Iversen LL, Iversen SD, Snyder SH, editors. Handbook of Psychopharmacology, Section 1, Vol 3. New York: Plenum Press; 1975. p. 381-442.
20. Friedgen B, Halbrügge T, Graefe K. Role of uptake$_1$ and catechol-O-methyltransferase in removal of circulating catecholamines in the rabbit. Am J Physiol Endocrinol Metab. 1994;267:E814-21.
21. Boudreau G, Péronnet F, de Champlain J, Nadeau R. Presynaptic effects of epinephrine on norepinephrine release from cardiac sympathetic nerves in dogs. Am J Physiol Heart Circ Physiol. 1993;265:H205-11.
22. Esler M, Jennings G, Lambert G, Meredith I, Horne M, Eisenhofer G. Overflow of catecholamine neurotransmitters to the circulation: source, fate, and functions. Physiol Rev. 1990;70:963-85.
23. Schmidt H, Schurr C, Hedler L, Majewski H. Local modulation of norepinephrine release in vivo: Presynaptic β_2-adrenoceptors and endogenous adrenaline. J Cardiovasc Pharmacol. 1984;6:641-9.
24. Kawada T, Sugimachi M, Shidhido T, Miyano H, Sato T, Yoshimura R, Miyashita H, Nakahara T, Alexander J Jr, Sunagawa K. Simultaneous identification of static and dynamic vagosympathetic interactions in regulating heart rate. Am J Physiol Regul Integr Comp Physiol. 1999;276:R782-9.
25. Kawada T, Miyamoto T, Uemura K, Kashihara K, Kamiya K, Sugimachi M, Sunagawa K. Effects of neuronal norepinephrine uptake blockade on baroreflex neural and peripheral arc transfer characteristics. Am J Physiol Regul Integr Comp Physiol. 2004;286:R1110-20.

ELSEVIER

Journal of Neuroscience Methods 156 (2006) 71–75

JOURNAL OF NEUROSCIENCE METHODS

www.elsevier.com/locate/jneumeth

Reversible vagal blockade in conscious rats using a targeted delivery device

Can Zheng [a,*], Toru Kawada [a], Meihua Li [a], Takayuki Sato [b], Kenji Sunagawa [c], Masaru Sugimachi [a]

[a] *Department of Cardiovascular Dynamics, Advanced Medical Engineering Center, National Cardiovascular Center Research Institute, 5-7-1 Fujishirodai, Suita-shi, Osaka 565-8565, Japan*

[b] *Department of Physiology, Kochi Medical School, Kochi 783-8505, Japan*

[c] *Department of Cardiovascular Medicine, Graduate School of Medical Sciences, Kyushu University, Fukuoka 812-8582, Japan*

Received 30 November 2005; received in revised form 7 February 2006; accepted 8 February 2006

Abstract

Reversible methods of nerve blockade greatly aid neurophysiological and behavioral studies. We have developed an implantable device for the local delivery of anesthetics to the area surrounding the vagal nerve in rats. The device consists of a thick silicone tube for insulating the nerves from the surrounding tissue, and a thin silicone tube for the infusion of anesthetics into the insulating tube. The in vivo performance of the device was tested electrophysiologically, and cardiovascular responses to vagal stimulation were measured in conscious animals. Nerve conductivity was completely blocked by injection of a small amount (<20 μl) of 1% lidocaine, with conductivity subsequently recovering gradually after 10–40 min. Electrical stimulation of the right vagus nerve in conscious rats increased arterial pressure while decreasing heart rate. The local blockade of afferent fibers abolished the arterial pressure response but preserved the bradycardic response to vagal nerve stimulation. The targeted delivery device was useful for reversible vagal blockade in conscious rats.

Keywords: Vagus; Conduction blockade; Electric stimulation; Heart rate; Blood pressure; Conscious; Rat

1. Introduction

Peripheral nerves are the first step in the pathway that conducts signals from various peripheral sensors to the central nervous system (CNS) and are also the output pathway for signals from the CNS to various organs, with most peripheral nerves containing both afferent and efferent fibers. In the investigation of the integrative functions of the autonomic nervous system, several techniques have been developed for performing nerve blockade for recording or selectively stimulating either afferent or efferent fibers. One such technique is surgical denervation, which effectively eliminates nerve conduction, but is irreversible and may not be applicable to the vagus nerve in the chronic experimental settings, as animals cannot survive for long after bilateral vagotomy. Nerve cooling provides a reversible nerve blockade in conscious large animals (Derksen et al., 1981; Borgdorff and Versteeg, 1984; Cudd, 1998) and in anesthetized small animals (Vizek et al., 1983; Schultz et al., 1988; Lee et al., 1990), but is difficult in conscious small animals such as rats, due to technical problems associated with the size of the nerve cooling device. Alternatively, local anesthetics such as lidocaine are widely used for nerve blockade in clinical practice and animal studies (Thalhammer et al., 1995; Gokin et al., 2001; Potocnik et al., 2001). The major advantages of anesthetics for nerve blockade are the complete reversibility of the nerve blockade and the ease of administration. However, it can be difficult to administer local anesthetics in small conscious animals, largely because the vagus nerve runs close to the common carotid artery and the aortic depressor nerve, and therefore the injection procedure may result in artery or nerve damage. A technique of delivering neurotrophins or anesthetics to the sciatic nerve has been demonstrated in the conscious rat model (Kanje et al., 1988; Costanzo et al., 1999). However, it is not yet known whether such a targeted delivery method can be used to block the vagus nerve in conscious rats. In this study, we designed a targeted delivery device for the rat vagus nerve, which allowed local

* Corresponding author. Tel.: +81 6 6833 5012x2427; fax: +81 6 6835 5403.
E-mail address: zhengcan@ri.ncvc.go.jp (C. Zheng).

0165-0270/$ – see front matter © 2006 Elsevier B.V. All rights reserved.
doi:10.1016/j.jneumeth.2006.02.015

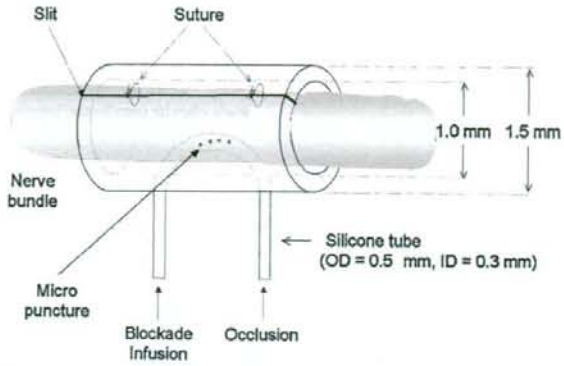

Fig. 1. Schematic illustration of the design of the targeted delivery device for the rat vagus nerve.

infusion of anesthetics into the area surrounding the nerve. The aim of this study was to evaluate this targeted delivery device for vagal blockade in conscious rats.

2. Materials and methods

2.1. A targeted delivery device

We designed an implantable device for delivering anesthetics to the area surrounding the rat cervical vagus nerve. As shown in Figs. 1 and 2E, this device was composed of a thick silicone tube (i.d. = 1.0 mm; o.d. = 1.5 mm; L = 3–4 mm) acting as a nerve guiding tube, and a thin silicone tube (i.d. = 0.3 mm; o.d. = 0.5 mm) for the injection of anesthetic agents. We made a longitudinal slit in the thick tube and pierced two holes in the wall of this tube for the thin tube to pass in and out of. Several micro-punctures were made by a microneedle (with a tip of 0.01 mm) in the inner part of the thin tube to allow the anesthetics to leak out into the guide tube.

We injected anesthetics slowly from one end of the thin tube until the liquid anesthetics replaced the air in the tube, and then we occluded the other end while increasing the pressure in the thin tube to force the liquid to leak out through the micro-punctures into the area surrounding the nerve. In the present study, we used 1% lidocaine solution for local blockade of vagal conduction. After completion of the experimental protocol, we flushed the tubes with distilled water to prevent the micro-punctures from becoming occluded by residual anesthetics.

2.2. Surgical preparation

Experiments were performed on six Sprague–Dawley rats weighing between 320 and 450 g. Animals were cared for in strict accordance with the Guiding Principles for the Care and Use of Animals in the Field of Physiological Science approved by the Physiological Society of Japan. Under 1.5%-halothane anesthesia, the lead wires of the cuff electrodes and the infusion tubes were tunneled subcutaneously from the back where they were fixed to a custom-designed multi-channel skin connector (Fig. 2B and G). The right vagus nerve was carefully dissected away from the common carotid artery and placed into the guide tube. The slit in the guide tube was then sutured by a polypropylene suture (8-0, ETHICON, INC.). Two custom-designed cuff electrodes, each having a pair of stainless steel wire electrodes (Fig. 2F), were implanted into the nerve trunk in the proximal and distal sides of the guide tube at a distance of 1.1–1.4 mm. Next, a blood pressure telemeter (TA11PA-C40, DSI) was implanted into the abdomen with a pressure sensor inserted into the abdominal aorta for monitoring mean arterial pressure (MAP) and heart rate (HR). After recovery from the surgical procedure, the animals were maintained on standard rat chow ad libitum, and were restrained in a rodent cage for physiological measurements as described below.

2.3. Experimental protocols

The experimental protocols were conducted at least 1 week after the implantation surgery. The in vivo effectiveness of the targeted delivery for nerve blockade was evaluated electrophysiologically and by measurement of HR and MAP responses to

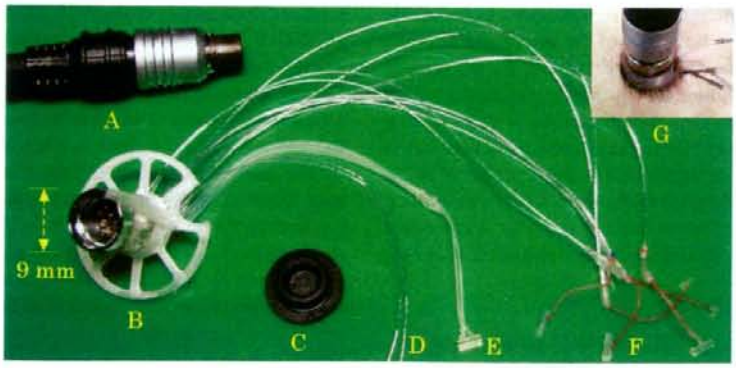

Fig. 2. Photographic images of the multi-channel skin connector with electrodes and nerve blocker. (A) Plug, (B) skin connector with 12-pin receptacle, (C) cap, (D) ECG leads, (E) nerve blocker, (F) nerve electrodes, the leads were extended with flexible coil (made of stainless wire of 0.03 mm in diameter, epoxy coated) and tips were fixed in the slit silicone tube (i.d. = 0.5; o.d. = 1 mm), and (G) implanted skin connector with local infusion setting.

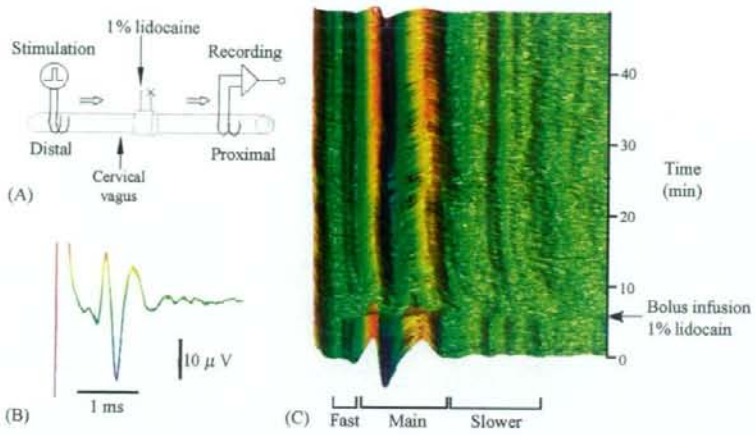

Fig. 3. Example of in vivo electrophysiology of the rat vagus. (A) A diagram of the experimental arrangement. (B) Compound action potential (CAP) of the right vagus evoked by the electrical pulse (1 Hz, 0.3 ms, 1.3 V). (C) The inhibition of vagal conduction by local injection of a small amount (<20 μl) of 1% lidocaine in conscious rats. Each trace was obtained as a result of waveform averaging of 10 single successive sweeps.

electrical stimulation of the vagus nerve in conscious animals. While the rat was loosely restrained in a rodent cage, lead wires for nerve stimulation and recording were attached to the skin connector (Fig. 2A and B). Arterial pressure was measured by telemetry. After carefully arranging the two electrodes and the delivery device, nerve stimulation with either distal or proximal nerve blockade was performed.

Nerve impulses were evoked by electrical stimulation of the vagus from the cuff electrode distal to the targeted delivery device (Fig. 3A). Rectangular pulses were delivered using a stimulator (SEN-7103, Nihon Kohden) and an isolator (SS-202J, Nihon Kohden). For in vivo electrophysiology, the stimulation frequency was 1 Hz and the pulse duration was 0.3 ms. The magnitude of stimulation was set at a supramaximal level (1.2–2.0 V). For functional experiments examining the AP and HR responses, the stimulation frequency, pulse duration, and magnitude were set at 10–30 Hz, 0.2–1 ms, and 2 V, respectively. The compound action potential (CAP) was amplified using an AC amplifier (200,000×, Model AB-610J, Nihon Kohden) with low (150 Hz) and high (1 kHz) frequency cutoffs. Nerve signals and arterial pressure data were sampled using a 12-bit A/D converter. Nerve signals were digitized at 5 kHz per electrode channel. The data were saved onto the hard disk of a dedicated laboratory computer system for later analysis.

2.4. Statistics

Data were reported as mean ± S.D. values. Changes in HR and MAP were compared before and during the stimulation by paired *t*-tests with the significance level set at $p < 0.05$.

3. Results

Fig. 3B shows the CAP of the vagus nerve evoked by electrical stimulation from the cuff electrode. The CAP consisted of one main component propagating at 0.9–2.1 m/s, as well as fast (>3 m/s) and slow (<0.9 m/s) components. All components of the CAP disappeared after an injection of a small amount (<20 μl) of 1% lidocaine (Fig. 3C). The fast component had almost recovered 15 min after the injection, followed by recovery of the main component in 40 min. The slow component required longer to recover.

The rats stayed quiet during the injection of anesthetics, with no changes in baseline HR and MAP. The HR and AP responses to electric stimulation differed after blockade of the afferent nerves, compared with before blockade. Prior to nerve blockade, electric stimulation of the right vagus nerve decreased HR abruptly, whereas it was associated with an increase in MAP, as shown in Fig. 4; HR decreased from 434 ± 8 to 246 ± 35 bpm ($p < 0.01$), whereas MAP increased from 99 ± 11 to 127 ± 14 mmHg ($p < 0.01$). However, after the blockade of afferent fibers, electrical stimulation of the nerve decreased HR without significant changes in MAP (HR 414 ± 4 bpm versus 266 ± 17 bpm, $p < 0.01$; MAP 106 ± 12 mmHg versus 103 ± 14 mmHg). The effects of vagal afferent blockade were

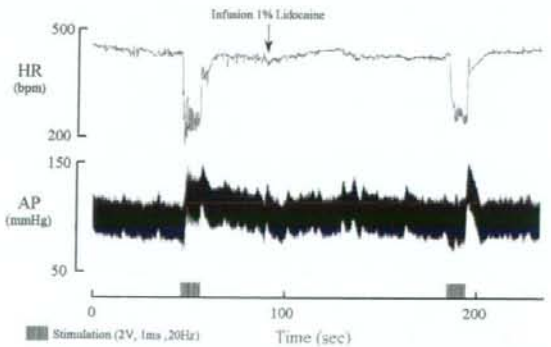

Fig. 4. Representative responses of arterial pressure (AP) and heart rate (HR) to electric stimulation (2 V, 1 ms, 20 Hz, 10 s) of the right vagus nerve before and after blockade of afferent fibers by local infusion of 1% lidocaine in conscious rats.

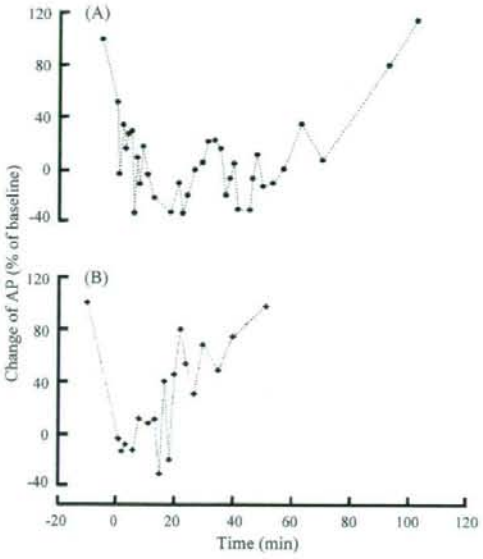

Fig. 5. Examples of the time course of the arterial pressure (AP) response to electric stimulation of cervical vagus nerve after afferent blockade by bolus infusion of 1% lidocaine in conscious rats. Each point represents the percentage of AP responses compared to the baseline response (before afferent blockade). Electric stimulations (2 V, 1 ms, 20 Hz, 10 s) were performed intermittently at interval greater than 1 min. The tests were done 1 week (A) and 2 weeks (B) after the implantation surgery.

reversible and the HR and MAP responses were restored in 15–60 min after the injection of 1% lidocaine. The duration of the nerve block was shorter in the second week than the first week (Fig. 5). The durability of the targeted delivery device was chiefly determined by how intact the infusion tube was. The effectiveness of the local blockade was confirmed 2 months after the implantation surgery.

4. Discussion

A variety of disease models, ranging from hypertension to heart failure, make the rat very important as an experimental animal for cardiovascular research. Reversible blockade of the autonomic nerves in small animals like the rat would be useful for physiological and behavioral study (Thalhammer et al., 1995), and would contribute to our understanding of the regulation of the cardiovascular system by the autonomic nervous system. We designed a targeted delivery device for the rat cervical vagus nerve. Using the targeted delivery device, in vivo electrophysiology and the functional evaluation of reversible nerve blockade were conducted in chronically instrumented, conscious rats. To our knowledge, this is the first study applying the targeted delivery device to blockade of the vagus nerve in conscious rats.

As shown in Fig. 3C, local injection of a small amount (<20 μl) of anesthetic (1% lidocaine) caused reversible, complete conduction block of the vagus nerve. The rats stayed calm in the rodent cage without any indication of significant stress during or after the injection of anesthetics. Temporary administration of anesthetics via the targeted delivery device lessens the stress compared to other techniques of nerve blockade requiring surgical procedures, and is therefore suitable for evaluating the role of the autonomic nervous system in circulatory regulation without significant sympathetic excitation associated with the stress. The infusion period and the type of anesthetics may control the duration of nerve blockade. For instance, lidocaine causes a relatively short-lived nerve blockade whereas marcaine causes a longer blockade. Selective anesthetics may also be used for vagal afferent blockade (Bowser-Riley et al., 1990). Fig. 5 shows that the duration of the nerve block lessoned over time after the implantation surgery even with the same dose of anesthetic. The space surrounding the nerve within the guide tube may be replaced by regenerated tissue over time after the surgical procedure, possibly reducing the effective volume of distribution for the anesthetic. Although vagal blockade has been reported to increase HR in large animals like ponies (Derksen et al., 1981), the vagal blockade did not increase baseline HR significantly in rats in the present study. The differences in the effects of vagal blockade on HR may be a result of species difference in basal vagal nerve activity.

The autonomic nerves usually contain both afferent and efferent fibers. Hence the selective stimulation or recording of either the afferent or efferent nerve is essential to assess the role of the autonomic nerves in circulatory regulation. Vagal afferent fibers conduct the signals from most of the organs in the thoracic and abdominal cavity to the medulla, stimulating various viscerogenic reflexes. Continuous electrical stimulation of the afferent fibers may exert intensity-dependent inhibition of breathing, anxiety, or even painful behavioral reactions, often accompanying the increase in arterial pressure. As shown in Fig. 4, prior to nerve blockade, right vagal stimulation decreased HR and increased MAP, and the increase in MAP was not observed after blocking the portion proximal to the stimulation electrodes, suggesting that the increase in MAP before the proximal blockade could be attributed to vagal afferent activation. Combining vagal afferent blockade with vagal stimulation, we were able to selectively evaluate the role of the vagal efferent function in conscious rats (Li et al., 2003).

In conclusion, we have demonstrated a reversible blockade of the vagus nerve in conscious rats. A complete conduction block was achieved by local administration of a minimal dose of anesthetics. The reversible nerve blockade can be combined with nerve stimulation or nerve recording techniques to stimulate or record the efferent or afferent autonomic nerve activity in conscious animals. This technique, involving the use of a targeted delivery device, has the potential to aid in furthering our understanding of the role of the autonomic nervous system in cardiovascular regulation, and to promote physiological and behavioral studies.

Acknowledgements

This study was supported by a "Health and Labour Sciences Research Grant for Research on Advanced Medical Technology" from the Ministry of Health, Labour and Welfare of Japan,

"Health and Labour Sciences Research Grant for Research on Medical Devices for Analyzing, Supporting and Substituting the Function of Human Body" from the Ministry of Health, Labour and Welfare of Japan, "Program for Promotion of Fundamental Studies in Health Science" from the National Institute of Biomedical Innovation, a Grant provided by the Ichiro Kanehara Foundation, "Ground-based Research Announcement for Space Utilization" promoted by Japan Space Forum, and "Industrial Technology Research Grant Program in 03A47075" from New Energy and Industrial Technology Development Organization (NEDO) of Japan.

References

Borgdorff P, Versteeg PG. An implantable nerve cooler for the exercising dog. Eur J Appl Physiol Occup Physiol 1984;53(2):175–9.

Bowser-Riley F, Cornish M, Kidd C, Zheng F. Role of vagal afferent C fibres in the bradycardiac response to an increase in arterial blood pressure in ferrets. Exp Physiol 1990;75(6):859–62.

Costanzo EM, Barry JA, Ribchester RR. Co-regulation of synaptic efficacy at stable polyneuronally innervated neuromuscular junctions in reinnervated rat muscle. J Physiol 1999;521(Pt 2):365–74.

Cudd TA. Vagal blockade does not prevent adrenocorticotropin, cortisol, and cardiopulmonary responses to thromboxane A2. Can J Physiol Pharmacol 1998;76(12):1087–94.

Derksen FJ, Robinson NE, Stick JA. Technique for reversible vagal blockade in the standing conscious pony. Am J Vet Res 1981;42(3):523–5.

Gokin AP, Philip B, Strichartz GR. Preferential block of small myelinated sensory and motor fibers by lidocaine: in vivo electrophysiology in the rat sciatic nerve. Anesthesiology 2001;95(6):1441–54.

Kanje M, Lundborg G, Edstrom A. A new method for studies of the effects of locally applied drugs on peripheral nerve regeneration in vivo. Brain Res 1988;439(1–2):116–21.

Lee LY, Morton RF, Kou YR. Acute effects of cigarette smoke on breathing in rats: vagal and nonvagal mechanisms. J Appl Physiol 1990;68(3):955–61.

Li M, Zheng C, Kawada T, Sato T. Vagal stimulation improved acute-phase survival after myocardial infarction in conscious rats. Circulation 2003;108(Suppl. IV):IV-268, 1268.

Potocnik I, Tomsic M, Bajrovic F. Sensitivity of sensory axons to lidocaine nerve block in rats. Pflugers Arch 2001;442(6 Suppl. 1):R193–4.

Schultz HD, Gardner DG, Deschepper CF, Coleridge HM, Coleridge JC. Vagal C-fiber blockade abolishes sympathetic inhibition by atrial natriuretic factor. Am J Physiol 1988;255(1 Pt 2):R6–13.

Thalhammer JG, Vladimirova M, Bershadsky B, Strichartz GR. Neurologic evaluation of the rat during sciatic nerve block with lidocaine. Anesthesiology 1995;82(4):1013–25.

Vizek M, Frydrychova M, Houstek S, Palecek F. Effect of vagal cooling on lung functional residual capacity in rats with pneumonia. Bull Eur Physiopathol Respir 1983;19(1):23–6.

Am J Physiol Heart Circ Physiol 291: H318–H326, 2006.
First published February 24, 2006; doi:10.1152/ajpheart.00975.2005.

Short-term electroacupuncture at Zusanli resets the arterial baroreflex neural arc toward lower sympathetic nerve activity

Daisaku Michikami,[1,2] Atsunori Kamiya,[1] Toru Kawada,[1] Masashi Inagaki,[1] Toshiaki Shishido,[1] Kenta Yamamoto,[1,2] Hideto Ariumi,[1,2] Satoshi Iwase,[3] Junichi Sugenoya,[3] Kenji Sunagawa,[4] and Masaru Sugimachi[1]

[1]*Department of Cardiovascular Dynamics, Advanced Medical Engineering Center, National Cardiovascular Center Research Institute, Osaka;* [2]*Pharmaceuticals and Medical Devices Agency, Tokyo;* [3]*Department of Physiology, School of Medicine Aichi Medical University, Nagakute, Aichi; and* [4]*Department of Cardiovascular Medicine, Kyushu University Graduate School of Medical Sciences, Fukuoka, Japan*

Submitted 12 September 2005; accepted in final form 17 February 2006

Michikami, Daisaku, Atsunori Kamiya, Toru Kawada, Masashi Inagaki, Toshiaki Shishido, Kenta Yamamoto, Hideto Ariumi, Satoshi Iwase, Junichi Sugenoya, Kenji Sunagawa, and Masaru Sugimachi. Short-term electroacupuncture at Zusanli resets the arterial baroreflex neural arc toward lower sympathetic nerve activity. *Am J Physiol Heart Circ Physiol* 291: H318–H326, 2006. First published February 24, 2006; doi:10.1152/ajpheart.00975.2005.—Although electroacupuncture reduces sympathetic nerve activity (SNA) and arterial pressure (AP), the effects of electroacupuncture on the arterial baroreflex remain to be systematically analyzed. We investigated the effects of electroacupuncture of Zusanli on the arterial baroreflex using an equilibrium diagram comprised of neural and peripheral arcs. In anesthetized, vagotomized, and aortic-denervated rabbits, we isolated carotid sinuses and changed intra-carotid sinus pressure (CSP) from 40 to 160 mmHg in increments of 20 mmHg/min while recording cardiac SNA and AP. Electroacupuncture of Zusanli was applied with a pulse duration of 5 ms and a frequency of 1 Hz. An electric current 10 times the minimal threshold current required for visible muscle twitches was used and was determined to be 4.8 ± 0.3 mA. Electroacupuncture for 8 min decreased SNA and AP ($n = 6$). It shifted the neural arc (i.e., CSP-SNA relationship) to lower SNA but did not affect the peripheral arc (i.e., SNA-AP relationship) ($n = 8$). SNA and AP at the closed-loop operating point, determined by the intersection of the neural and peripheral arcs, decreased from 100 ± 4 to 80 ± 9 arbitrary units and from 108 ± 9 to 99 ± 8 mmHg (each $P < 0.005$), respectively. Peroneal denervation eliminated the shift of neural arc by electroacupuncture ($n = 6$). Decreasing the pulse duration to <2.5 ms eliminated the effects of SNA and AP reduction. In conclusion, short-term electroacupuncture resets the neural arc to lower SNA, which moves the operating point toward lower AP and SNA under baroreflex closed-loop conditions.

arterial pressure; equilibrium diagram

ALTHOUGH THERE ARE MANY clinical case reports (21, 30, 32, 39, 40, 42), the effects of electroacupuncture on cardiovascular regulation remain to be systematically investigated. There has been a recent renewal of interest in the inhibitory effects of electroacupuncture of the Zusanli acupoint on the cardiovascular system, including reductions in arterial pressure (AP), heart rate, (3, 15, 16), and sympathetic nerve activity (SNA) (25, 42). Such inhibitory effects are observed during low-frequency (<20 Hz) electroacupuncture. Because the arterial baroreflex is one of the most important control systems that stabilize AP, we quantified the effects of electroacupuncture on the arterial baroreflex over an entire operating range. Systematic analysis would help to assess the possible utility of electroacupuncture as a treatment modality for certain cardiovascular diseases with vagolytic and sympathotonic states (26, 38).

One of the best ways to quantitatively analyze changes in the arterial baroreflex over an entire operating range may be analysis using a baroreflex equilibrium diagram (10, 23, 31) (see APPENDIX for details). Briefly, the baroreflex equilibrium diagram consists of a neural arc representing SNA as a function of baroreceptor input pressure and a peripheral arc representing AP as a function of SNA. The intersection of the two arcs corresponds to an operating point of the AP regulation under baroreflex closed-loop conditions. Considering the reduced AP and SNA found in previous studies, we hypothesized that short-term electroacupuncture resets the arterial baroreflex neural arc to lower SNA. In the present study, to test this hypothesis, we constructed a baroreflex equilibrium diagram with neural and peripheral arcs in anesthetized rabbits. The present findings indicate that electroacupuncture resets the baroreflex neural arc to lower SNA, moving the closed-loop operating point toward lower AP and SNA.

MATERIALS AND METHODS

Surgical Preparation

Animals were cared for in strict accordance with the *Guiding Principles for the Care and Use of Animals in the Field of Physiological Sciences* approved by the Physiological Society of Japan. Twenty-two Japanese White rabbits weighing 2.4–3.3 kg were anesthetized via intravenous injection (2 ml/kg) with a mixture of urethane (250 mg/ml) and α-chloralose (40 mg/ml) and mechanically ventilated with oxygen-enriched room air. Supplemental doses were injected as necessary (0.5 ml/kg) to maintain an appropriate level of anesthesia. Body temperature was maintained at ~38°C with a heating pad. AP was measured by using a high-fidelity pressure transducer (SPC-330A, Millar Instruments, Houston, TX) inserted via the left femoral artery. To record cardiac SNA, we exposed the left cardiac sympathetic nerve through a midline thoracotomy and attached a pair of stainless steel wire electrodes (Bioflex wire AS633, Cooner Wire, Chatsworth, CA) to the nerve. The nerve fibers peripheral to the

Address for reprint requests and other correspondence: D. Michikami, Dept. of Cardiovascular Dynamics, Advanced Medical Engineering Center, National Cardiovascular Center Research Institute, 5-7-1 Fujishirodai, Suita, Osaka 565–8565, Japan (e-mail: dmichi@ri.ncvc.go.jp or kamiya@ri.ncvc.go.jp).

The costs of publication of this article were defrayed in part by the payment of page charges. The article must therefore be hereby marked "*advertisement*" in accordance with 18 U.S.C. Section 1734 solely to indicate this fact.

electrodes were sectioned to eliminate afferent signals from the heart. To insulate and fix the electrodes, the nerves and electrodes were secured with silicone glue (Kwik-Sil, World Precision Instruments, Sarasota, FL). The preamplified nerve signals were band-pass filtered at 150–1,000 Hz, full-wave rectified, and low-pass filtered at a cutoff frequency of 30 Hz by using analog circuit. After that, the neural signals were recorded at a sampling rate of 200 Hz using a 12-bit analog-to-digital converter. Pancuronium bromide (0.1 mg/kg) was administered to prevent contaminating muscular activities. At the end of the experiment, the experimental animals were killed by an overdose of intravenous pentobarbital sodium, and the background noise level of SNA was determined postmortem.

Sixteen of the 22 rabbits were used in *protocol 1 (protocols 1-1, 1-2, and 1-3)*, and the remaining 6 rabbits were used in *protocols 2, 3,* and *4*. In 10 of the 16 rabbits for *protocols 1-2* and/or *1-3* described below, we isolated both carotid sinuses from the systemic circulation by ligating the internal and external carotid arteries and other small branches originating from the carotid sinus regions. The isolated carotid sinuses were filled with warmed physiological saline through catheters inserted via the common carotid arteries. The intra-carotid sinus pressure (CSP) was controlled by a servo-controlled piston pump (model ET-126A, Labworks, Costa Mesa, CA). In the baroreflex open-loop experimental settings, bilateral vagal and aortic depressor nerves were sectioned at the neck to minimize reflex effects from cardiopulmonary regions and the aortic arch.

Electroacupuncture

Two stainless steel needles were inserted at the one-fifth point (from the knee) and the midpoint of the knee-ankle distance of approximately 30–35 mm. These needles with a diameter of 0.2 mm (CE0123, Seirin-Kasei, Shimizu City, Japan) were inserted to a depth of ~10 mm in the skin and underlying muscle (the right tibialis anterior muscle). This area corresponds to the Zusanli and Xiajuxu acupoints (over the peroneal nerve below the knee, stomach meridian, St 36 and 39) in humans.

As in previous studies (2, 3, 17, 42), the stimulus current intensity was determined as 10 times of twitch threshold, which is the minimal electrical current required for eliciting visible muscle twitches of the stimulated leg. Actually, the current was 4.8 ± 0.3 mA (4.2–5.4 mA). An electric rectangular wave current with a frequency of 1 Hz and with pulse duration of 5 ms was passed between these two needles by using an electrical stimulator (SEN-7203, Nihon Kohden) except *protocol 4* where shorter pulse durations were challenged.

Protocols

The experimental protocol was approved by the Animal Experimental Committee of National Cardiovascular Center Research Institute.

Protocol 1: effect of Zusanli electroacupuncture on AP, SNA, and baroreflex. PROTOCOL 1-1 (BAROREFLEX CLOSED-LOOP CONDITION, N = 6). To elucidate the overall cardiovascular inhibitory effects of electroacupuncture, we performed 1 Hz electroacupuncture for 8 min and measured AP and SNA responses under conditions of intact cardiovascular reflexes. In this closed-loop protocol, vagal and aortic depressor nerves were preserved. Baseline data were measured for 1 min before acupuncture insertion. At 10 min after acupuncture insertion, baseline data were measured again for 1 min. Electroacupuncture was applied for 8 min. The recovery data were measured for 2 min after the cessation of electroacupuncture.

PROTOCOL 1-2 (BAROREFLEX OPEN-LOOP CONDITION, N = 8). To elucidate the effects of electroacupuncture on the arterial baroreflex over an entire operating range, we performed a baroreflex open-loop experiment as follows. CSP was first decreased to 40 mmHg. After attainment of a steady state, CSP was increased from 40 to 160 mmHg in increments of 20 mmHg. Each pressure step was maintained for 60 s. We measured AP and SNA during the stepwise increase in CSP. Two trials (control and electroacupuncture trials) were performed on each rabbit. The order of the trials was randomized. The electroacupuncture trial was identical to the control trial except that electroacupuncture was commenced 1 min before the initiation of stepwise increase in CSP.

PROTOCOL 1-3 (BAROREFLEX OPEN-LOOP CONDITION WITH PERONEAL DENERVATION, N = 6). To identify the afferent pathway of electroacupuncture, we examined the effects of 1 Hz electroacupuncture on the arterial baroreflex after severing the right peroneal nerve at the level of the knee joint. Estimation of the baroreflex equilibrium diagram was conducted as in *protocol 1-2* in the control and electroacupuncture trials. Four of the six rabbits had also undergone *protocol 1-2*.

Protocol 2: effects of sham (nonelectrical) acupuncture at Zusanli and control (nonspecific) electrical and nonelectrical acupunctures on AP and SNA in baroreflex closed-loop condition (n = 6). To determine whether changes in AP and SNA during Zusanli electroacupuncture are specific responses, sham and control acupunctures were conducted under the following acupuncture conditions: *1*) no acupuncture (nonacupuncture), *2*) nonelectrical acupuncture at Zusanli-Xiajuxu (St 36–39) acupoints (sham acupuncture), *3*) nonelectrical acupuncture at Guangming-Xuanzhong (gallbladder meridian, Gb 37–39) acupoints (control acupuncture), and *4*) electrical acupuncture at Guangming-Xuanzhong acupoints (control electroacupuncture). We chose Guangming-Xuanzhong as nonspecific control acupoints (*trials 3* and *4*) because these acupoints are believed to reduce leg pain without affecting the cardiovascular system, in contrast to the Zusanli-Xiajuxu acupoints. In each trial, AP and SNA were measured for a baseline duration of 1 min, under acupuncture condition (*trial 1, 2, 3,* or *4*) for 8 min, and recovery for 1 min.

Protocol 3: effect of long-term Zusanli electroacupuncture on AP and SNA in baroreflex closed-loop condition (n = 6). To clarify the effect of long-term electroacupuncture on cardiovascular system, AP and SNA were measured during and after 30 min of electroacupuncture at Zusanli-Xiajuxu acupoints. *Protocol 3* was conducted in the same manner as *protocol 1-1* except with a longer stimulation duration than *protocol 1-1* (8 min).

Protocol 4: Effect of pulse duration of Zusanli electroacupuncture on AP and SNA in baroreflex closed-loop condition (n = 6). To examine the effect of pulse duration of electroacupuncture on AP and SNA, AP and SNA were measured during electroacupuncture at Zusanli-Xiajuxu acupoints with the pulse duration increasing stepwise from 0.1 to 0.25, 0.5, 1, 2.5, 5, and 10 ms, every 60 s. In each animal, the frequency and stimulus current intensity were maintained constant as in *protocols 1, 2,* and *3*.

Data Analysis

We recorded CSP, SNA, and AP at a sampling rate of 200 Hz by using a 12-bit analog-to-digital converter. Data were stored on the hard drive of a dedicated laboratory computer system for later analyses.

In *protocol 1-1, 2, and 4*, mean AP and SNA for 1 min were calculated for baseline conditions, every minute of electroacupuncture, and recovery. In *protocol 3*, mean AP and SNA for 5 min were calculated for baseline conditions, electroacupuncture, and recovery. In *protocols 1-2* and *1-3*, we calculated mean AP and SNA during the last 10 s of each CSP step. Because the absolute magnitude of SNA depended on recording conditions, SNA was presented in arbitrary units (au). The background noise level was set at 0 au and the SNA value at the closed-loop operating point in the control trial (without electroacupuncture) was set at 100 au for each animal.

A four-parameter logistic function analysis was performed on the neural arc (CSP-SNA data pairs) and the peripheral arc (SNA-AP data pairs) as follows (11)

$$y = \frac{P_1}{1 + \exp[P_2(x - P_3)]} + P_4 \qquad (1)$$

where x and y represent the input and the output, respectively. P_1 denotes the response range (i.e., the difference between the maximum and minimum values of y), P_2 is the coefficient of gain, P_3 is the midpoint of the logistic function on the input axis, and P_4 is the minimum value of y. The maximum gain (G_{max}) is calculated from $-P_1P_2/4$ at $x = P_3$. The parameter values were calculated by an iterative nonlinear least-squares regression known as the downhill simplex method.

Statistical Analysis

All data are presented as means ± SD. Differences were considered to be significant when $P < 0.05$. In *protocols 1-1, 2, 3,* and *4*, the effects of electroacupuncture on AP and SNA at different time intervals were evaluated by one-way ANOVA. The Dunnett's test was used for multiple comparisons. In *protocols 1-2* and *1-3*, the effects of electroacupuncture on the four parameters of the logistic functions relating to the neural and peripheral arcs, as well as on the closed-loop operating point, were examined by using a paired *t*-test.

RESULTS

Figure 1*A* (*protocol 1-1*) shows a typical time series of AP and SNA in response to Zusanli-Xiajuxu electroacupuncture with intact cardiovascular reflexes. AP and SNA were reduced immediately after beginning electroacupuncture, and these remained reduced during 8-min electroacupuncture. Figure 1*B* illustrates the group-averaged AP and SNA in response to electroacupuncture. AP and SNA for baseline were unchanged by acupuncture insertion alone, while these values for 8-min electroacupuncture remained decreased from baseline. These values returned to baseline level after the cessation of electroacupuncture.

Figure 2 (*protocol 1-2*) shows a typical AP and SNA response to the increments in CSP in the control (Fig. 2, *left*) and electroacupuncture (Fig. 2, *right*) trials. A stepwise increase in CSP decreased SNA and AP in both trials. In the electroacupuncture trial, the AP and SNA response ranges to CSP were attenuated compared with the control trial.

Figure 3, *A* and *B* (*protocol 1-2*), shows the averaged baroreflex neural and peripheral arcs obtained in control and electroacupuncture trials. The neural arc showed a sigmoidal relationship between CSP and SNA. In the neural arc, the response range of SNA (P_1) and midpoint of the operating range (P_3) were significantly decreased by electroacupuncture (Table 1). The coefficient of gain (P_2), the minimum value of SNA (P_4), and G_{max} did not differ between the two trials (Table 1). As a result, the maximum value of SNA, calculated from $P_1 + P_4$, was significantly decreased by electroacupuncture from 162 ± 31 to 130 ± 29 au ($P < 0.005$). The peripheral arc showed a more linear relationship between SNA and AP than the neural arc. In the peripheral arc, electroacupuncture did not affect any of the four parameters or G_{max} (Table 1 and Fig. 3*B*). The operating point determined by the intersection of the neural and peripheral arcs was moved toward lower AP and SNA (from *point a* to *point b*) by electroacupuncture (Fig. 3*C* and Table 1).

Figure 4 (*protocol 1-3*) shows the averaged baroreflex neural (Fig. 4*A*) and peripheral arcs (Fig. 4*B*) in control and electroacupuncture trials with severance of the peroneal nerve innervating the tibialis anterior muscle. Two arcs obtained in both trials were nearly superimposable. The four parameters and G_{max} in the neural and peripheral arcs and operating point were

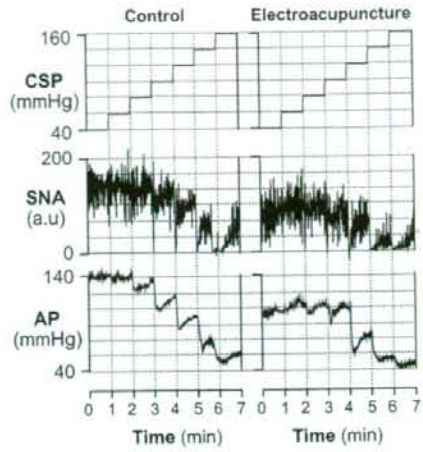

Fig. 2. Typical time series of intra-carotid sinus pressure (CSP), AP, and SNA in control (*left*) and electroacupuncture trials (*right*) in *protocol 1-2*. SNA and AP decreased in response to increments in CSP in both of the two trials. The response ranges of AP and SNA to CSP were lower in electroacupuncture than in controls.

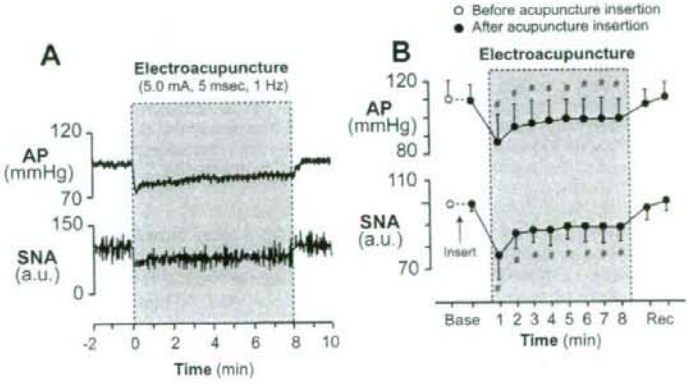

Fig. 1. Typical time series of arterial pressure (AP) and sympathetic nerve activity (SNA) during 8 min of 1-Hz electroacupuncture (*A*) and the averaged ($n = 6$) AP and SNA (*B*) in *protocol 1-1*. Data include periods of baseline (Base, 1 min), electroacupuncture (8 min), and recovery (Rec, 1 min). Each data point represents average values over 1 min. #$P < 0.05$: significantly different from baseline after acupuncture insertion. au, Arbitrary units.

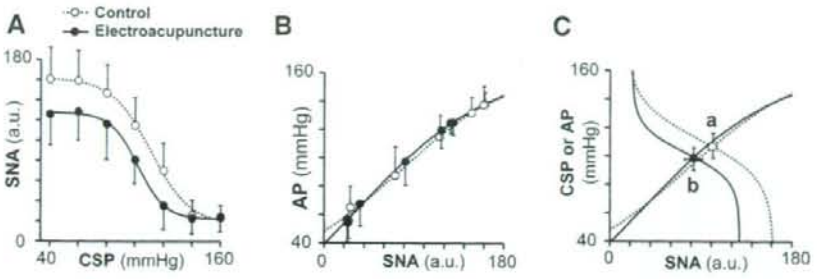

Fig. 3. Averaged (n = 8) baroreflex neural arc (A), peripheral arc (B), and baroreflex equilibrium diagram (C) obtained in 8 rabbits in control (○) and electroacupuncture (●) trials in *protocol 1-2*. Electroacupuncture shifted the neural arc to lower SNA (A), but it did not change the peripheral arc (B). The shift in neural arc reduced AP and SNA by 9 ± 3 mmHg and 20 ± 10 au (from *point a* to *point b*) at the operating point (C).

not affected by electroacupuncture when the peroneal nerve was denervated (Table 2 and Fig. 4*C*).

Figure 5 (*protocol 2*) shows the changes in AP and SNA during nonacupuncture (without acupuncture), sham acupuncture [nonelectrical acupuncture at Zusanli-Xiajuxu (St 36–39)], control acupuncture [nonelectrical acupuncture at Guangming-Xuanzhong (Gb 37–39)] and control electroacupuncture (electrical acupuncture at Gb 37–39) trials. AP and SNA did not change in these trials.

Figure 6, *A* and *B* (*protocol 3*), shows a typical time series and the averaged data, respectively, of AP and SNA in response to long-term Zusanli-Xiajuxu electroacupuncture. AP and SNA decreased immediately after electroacupuncture was started and remained reduced during 30-min electroacupuncture. In addition, AP and SNA returned to the preelectroacupuncture baseline levels immediately after cessation of electroacupuncture.

Figure 7, *A* and *B* (*protocol 4*), shows a typical time series and the averaged data, respectively, of AP and SNA during Zusanli-Xiajuxu electroacupuncture with the pulse duration increasing from 0.1 to 5 ms. Although increasing the pulse duration from 0.1 to 1 ms did not change AP and SNA, pulse durations of 2.5 ms and higher decreased SNA while pulse durations of 5 and 10 ms decreased AP.

Table 1. *Effect of electroacupuncture on the operating point of baroreflex and on the 4 parameters of logistic functions approximating neural and peripheral baroreflex arcs*

	Control	Electroacupuncture
Operating point		
Arterial pressure, mmHg	108.4±8.7	98.8±7.9†
Sympathetic nerve activity, au	99.8±4.1	80.0±8.9†
Neural arc		
P_1, au	144.0±35.0	112.6±9.2†
P_2, au/mmHg	0.08±0.03	0.09±0.09
P_3, mmHg	111.4±6.5	103.3±10.0*
P_4, au	17.5±6.1	17.4±8.7
G_{max}, au/mmHg	−2.94±0.91	−2.58±1.27
Peripheral arc		
P_1, mmHg	129.6±20.5	125.9±19.5
P_2, au/mmHg	−0.03±0.01	−0.03±0.01
P_3, au	80.6±23.2	71.7±17.1
P_4, mmHg	29.9±16.3	29.5±12.1
G_{max}, mmHg/au	0.74±0.10	0.84±0.18

Values are means ± SD (n = 8). G_{max}, maximum gain. See *Data Analysis* for definition of 4 parameters of logistic function. au, Arbitrary units. *P < 0.05 and †P < 0.005 vs. control.

DISCUSSION

The major new finding of the present study was that electroacupuncture at Zusanli resets the arterial baroreflex neural arc to lower SNA but does not significantly affect the baroreflex peripheral arc. As a result, the operating point determined by the intersection of the neural and peripheral arcs was moved toward lower SNA and AP by electroacupuncture. To the best of our knowledge, this is the first study delineating the effects of short-term electroacupuncture on the arterial baroreflex over an entire operating range.

Effects of Electroacupuncture on the Arterial Baroreflex (Protocol 1)

The arterial baroreflex system is one of the most important negative-feedback systems that stabilize AP against exogenous disturbances. When AP is decreased by exogenous perturbation such as blood loss, the reduction in AP is sensed by the arterial baroreceptors. SNA is then increased by the arterial baroreflex to buffer the reduction in AP. In such circumstances, SNA and AP change reciprocally. On the other hand, when SNA is changed by an exogenous perturbation such as emotional stress, SNA and AP change in parallel. In *protocol 1-1*, electroacupuncture decreased both SNA and AP, indicating that electroacupuncture introduced exogenous perturbation to decrease SNA with a resultant reduction in AP. Although the net effect of electroacupuncture is to decrease SNA, the perturbation of AP cannot be excluded. For example, because electroacupuncture also twitched the hindlimb muscles, electroacupuncture might have perturbed AP via changes in vascular resistance and/or venous return through muscle pump function. Therefore, to quantify the contribution of both perturbations on SNA and on AP, we performed *protocol 1-2*. Perturbation of AP is most easily detected by comparing AP at the same SNA level with and without electroacupuncture.

In *protocol 1-2*, we performed a baroreflex open-loop experiment and identified the static characteristics of the neural and peripheral arcs over a wide operating range. As expected, electroacupuncture shifted the neural arc toward lower SNA and decreased maximum SNA to ~80% of control (Fig. 3*A*). This shift is not due to reduced perfusion to the medulla by AP reduction during electroacupuncture because the AP was decreased by ~10 mmHg and would not induce cerebral ischemia. In contrast, electroacupuncture had little effect on the peripheral arc (Fig. 3*B*). In other words, AP with and without electroacupuncture did not differ significantly at any of the SNA levels. Therefore, changes in AP observed in *protocol 1-1*

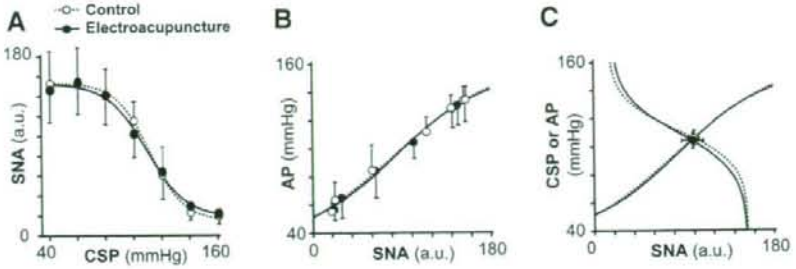

Fig. 4. Averaged (n = 6) baroreflex neural arc (A), peripheral arc (B), and baroreflex equilibrium diagrams (C) obtained in 6 rabbits in control (○) and electroacupuncture (●) trials with peroneal denervation in *protocol 1-3*. The baroreflex neural arc, peripheral arc, and the operating point were not influenced by electroacupuncture after peroneal denervation.

were attributable exclusively to perturbation of SNA and not to possible perturbation effects of electroacupuncture on AP.

The neural and peripheral arcs were combined to yield a baroreflex equilibrium diagram (Fig. 3*C*). The closed-loop operating point, determined by the intersection of the neural and peripheral arcs, moved from *point a* to *point b* during electroacupuncture. Despite a significant shift in the closed-loop operating point, neither the neural nor peripheral arc gain was altered significantly (Table 1). The fact that the baroreflex gain was maintained during electroacupuncture suggests the possible application of electroacupuncture to the treatment of cardiovascular diseases with sympathetic hyperactivity. However, the preservation of the arterial baroreflex gain in the present experimental settings may rely on normal peripheral arc characteristics. Cardiovascular diseases such as heart failure may decrease the peripheral arc gain to a variable extent due to impaired pump function. Whether the arterial baroreflex function during electroacupuncture can be maintained in cardiovascular diseases awaits future study.

Mechanisms for the Cardiovascular Inhibitory Effects of Electroacupuncture (Protocol 1)

The resetting in the baroreflex neural arc during electroacupuncture was mediated by a somatosympathetic reflex arising from the stimulated hindlimb, as evidenced by the fact that peroneal denervation abolished the resetting (Table 2 and Fig. 4). This result was consistent with an earlier study (27) showing that depressor and sympathoinhibitory responses during acupuncture were abolished by sciatic and femoral denervation. The existence of a somatosympathetic reflex is also supported by the fact that electrical stimulation of somatic afferents reduced AP (7–9). Legramante et al. (14) showed that rapidly conducting group III somatic afferent activation can evoke AP reduction during 1-Hz electrical stimulation of the tibial nerve. In contrast, high-frequency stimulation of the somatic afferent evokes AP elevation. Passive muscle stretching, which is considered to activate group III somatic afferent fibers, shifts the baroreflex neural arc toward higher SNA, resulting in an increase in the closed-loop operating point (41). The mechanism of two opposing influences of somatic afferent activation depending on the stimulation frequency is not fully understood.

Table 2. *Effect of electroacupuncture with peroneal denervation on the operating point of baroreflex and on the 4 parameters of logistic functions approximating neural and peripheral baroreflex arcs*

	Control	Electroacupuncture
Operating point		
Arterial pressure, mmHg	105.7±5.7	104.1±5.6
Sympathetic nerve activity, au	99.8±5.1	98.3±11.1
Neural arc		
P_1, au	138.3±42.4	136.3±38.6
P_2, au/mmHg	0.11±0.03	0.08±0.03
P_3, mmHg	112.7±10.2	111.5±10.6
P_4, au	14.9±8.7	15.7±7.4
G_{max}, au/mmHg	−3.27±1.15	−2.84±1.12
Peripheral arc		
P_1, mmHg	144.1±35.5	140.5±34.4
P_2, au/mmHg	−0.02±0.002	−0.02±0.004
P_3, au	82.0±34.0	78.8±32.0
P_4, mmHg	26.1±8.1	25.5±5.3
G_{max}, mmHg/au	0.69±0.13	0.72±0.21

Values are means ± SD (n = 6). See *Data Analysis* for definition of 4 parameters of logistic function.

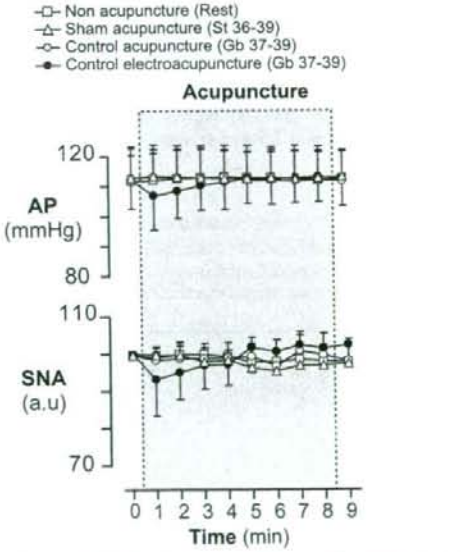

Fig. 5. Averaged (n = 6) AP (*top*) and SNA (*bottom*) in nonacupuncture (condition without acupuncture, □), sham acupuncture [nonelectrical acupuncture at Zusanli-Xiajuxu (stomach meridian, St 36–39), △], control acupuncture [nonelectrical and acupuncture at Guangming-Xuanzhong (gallbladder meridien, Gb 37–39), ○], and control electroacupuncture [electrical acupuncture at Gb 37–39, ●] trials in *protocol 2*. Data include periods of baseline (1 min), electroacupuncture (8 min), and recovery (1 min). Each data point represents average values over 1 min.